# Contribution of proton precipitation to space-based auroral FUV observations

M. Galand
Center for Space Physics, Boston University, Boston, Massachusetts, USA

D. Lummerzheim
Geophysical Institute, University of Alaska, Fairbanks, Alaska, USA

Received 14 November 2003; revised 17 December 2003; accepted 23 January 2004; published 27 March 2004.

[1] Imaging from space offers a unique way to access the global picture, and its temporal variability, of the particle energy input over the auroral ovals. Electron characteristics are inferred from the analysis of auroral images taken from space in two different spectral bands in UV or visible. Usually, only the electron component of the precipitation is considered, as most of the particle energy is carried by electrons. However, at some locations and certain times protons are a major energy source, that is, a major ionization and excitation source of the atmosphere. The response of POLAR/UVI, IMAGE/WIC and SI13, and TIMED/GUVI (used for retrieving the electron components) to proton precipitation is estimated. Secondary electrons produced within the proton beam also contribute to auroral emissions. Since they are less energetic than the secondary electrons produced in electron aurora, they have a different spectral signature. In addition, for a given energy flux, protons are usually more efficient at ionizing than electrons and yield larger values of the Pedersen ionospheric conductance. Therefore the difference between proton and electron aurora can lead to misinterpretation when brightness ratios are used to derive ionospheric conductances with parameterizations that are based on electron aurora. The validation and limitations of auroral analysis are discussed, especially at the equatorward edge of the afternoon oval, where protons are a significant energy source. In regions of >4 keV electron precipitation, the presence of proton precipitation, even modest ($\sim$10%), yields a large underestimation of both the electron mean energy and the energy flux. Overall, the presence of proton precipitation yields a poor estimation of the electron mean energy. In proton-dominated aurora, the Pedersen and Hall conductances are always underestimated with a large discrepancy for POLAR/UVI. However, in location where the protons are not dominant and the electron precipitation is not too hard, it is legitimate to estimate the particle characteristics and ionospheric conductances from the FUV brightnesses assuming pure electron precipitation. This is true in particular for the period around midnight (1900–0400 MLT), at a magnetic latitude of 65–67°. *INDEX TERMS:* 2455 Ionosphere: Particle precipitation; 2407 Ionosphere: Auroral ionosphere (2704); 2423 Ionosphere: Ionization mechanisms; 2447 Ionosphere: Modeling and forecasting; *KEYWORDS:* auroral protons, FUV

**Citation:** Galand, M., and D. Lummerzheim (2004), Contribution of proton precipitation to space-based auroral FUV observations, *J. Geophys. Res.*, *109*, A03307, doi:10.1029/2003JA010321.

## 1. Introduction

[2] Auroral particle precipitation is an important energy source which affects the electrodynamic properties, dynamics, and thermal structures, as well as the constituent distribution at the high-latitude, lower thermosphere region. Most of the auroral particle energy is carried into the ionosphere by energetic electrons [e.g., *Fuller-Rowell and Evans*, 1987; *Rees et al.*, 1995]. There are, however, regions where protons in the keV energy range are the dominant energy source upon the ionosphere. This is the case at the equatorial edge of the afternoon auroral oval [e.g., *Hardy et al.*, 1989]. In such a region, protons significantly contribute to the *E* region ionization and electrical ionospheric conductances [e.g., *Galand et al.*, 2001, and references therein].

[3] The only way to get global snapshots of the particle input over the entire auroral oval is through space-based auroral imaging. Past and recent missions (e.g., Dynamics Explorer (DE)-1, POLAR, Imager for Magnetopause-to-Aurora Global Exploration (IMAGE), Thermosphere Ionosphere Mesosphere Energetics Dynamics (TIMED)) have


0148-0227/04/2003JA010321$09.00

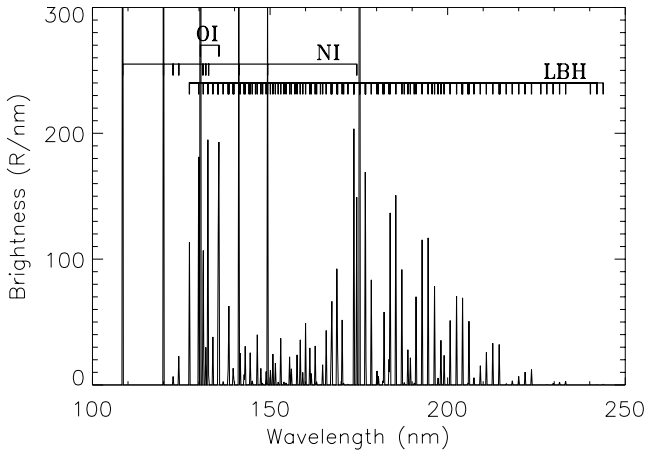


**Figure 1.** Modeled FUV spectrum produced by an incident electron flux of Maxwellian distribution with a mean energy of 4 keV and an energy flux of 1 mW $m^{-2}$.

used X-rays, far ultraviolet (FUV), and visible auroral images to retrieve the characteristics of the electron precipitation and to assess the response of the ionosphere/thermosphere system to the electron forcing on a global scale. In the visible and FUV ranges the mean energy of the incident electrons is retrieved from the brightness ratio in two different wavelength regions while the incident energy flux is retrieved from the total brightness in a given spectral window [e.g., *Lummerzheim et al.*, 1997; *Germany et al.*, 1997; *Frank et al.*, 1995; *Frey et al.*, 2002]. Such information over the entire auroral oval is crucial for assessing the ionospheric state [*Rees et al.*, 1995], for estimating the overall energy budget during a magnetic cloud event [*Lu et al.*, 1998], and for studying the magnetospheric source regions of auroral precipitation and field-aligned currents during a substorm [*Lu et al.*, 2000]. In such analyses, often the proton component of the precipitation is neglected or poorly estimated. In certain regions of the auroral oval, energetic protons make a significant contribution to, even dominate, the visible and FUV aurora [*Frey et al.*, 2001; 2002; *Lummerzheim et al.*, 2001; *Galand et al.*, 2002]. The presence of proton aurora can upset the values of brightnesses and brightness ratios derived from pure electron aurora that are used to estimate the electron characteristics and ionospheric conductances.

[4] In this paper we assess the contribution of energetic protons to the FUV emissions used to retrieve the electron mean energy and energy flux from POLAR/Ultraviolet Imager (UVI), TIMED/Global Ultraviolet Imager (GUVI), and IMAGE/Far Ultraviolet Imager (FUV) instruments. We address this goal by conducting several computer experiments based on a combined, comprehensive electron and proton transport model. We estimate the influence of proton precipitation on the assessment of the electron mean energy, total energy flux, and perpendicular ionospheric conductances, when these physical quantities are derived from the FUV brightnesses assuming pure electron precipitation. We apply this approach to Tromsø, Norway (69.6°N, 19.2°E geographic and 66.4°N, 103.4°E geomagnetic coordinates), which moves under a region of intense proton precipitation in the afternoon sector [e.g., *Senior*, 1991; *Lilensten and Galand*, 1998; *Galand et al.*, 2003; M. Galand et al., Spectral imaging of proton aurora and twilight at Tromsø, Norway, submitted to *Journal of Geophysical Research*, 2004], for a magnetic activity of $K_p = 4$. The misinterpretation of the FUV brightnesses to derive the electron characteristics is also evaluated in the midnight sector at Tromsø as well as at Poker Flat, Alaska (65.1°N, 212.5°E geographic and 65.2°, 263.2°E geomagnetic coordinates), another location of intense proton precipitation in the afternoon sector [*Basu et al.*, 1987; *Senior et al.*, 1987; *Deehr and Lummerzheim*, 2001; *Lummerzheim and Galand*, 2001]. Finally, we review our primary results and discuss how the proton component of the precipitation can be taken into account. We use the term "electron aurora" and "proton aurora" exclusively to distiguish the type of particle precipitation. Both types of aurora have the full spectrum of auroral emissions, and the proton aurora has in addition Doppler-shifted hydrogen emissions.

## 2. Retrieving the Electron Mean Energy and Energy Flux From FUV Brightnesses

[5] Figure 1 shows a modeled FUV spectrum produced in electron aurora. This spectrum is provided by a comprehensive electron transport model, as described in section 3.1. The incident electron flux is chosen to be a Maxwellian with a mean energy of 4 keV and an energy flux of 1 mW $m^{-2}$. The top of the atmosphere is chosen to be at 600 km. The dominant emission feature of the FUV spectrum in electron aurora is the $N_2$ Lyman-Birge-Hopfield (LBH) system spreading from 127.3 nm to 255.5 nm and associated with the transition between the $a^1\Pi_g$ state and the ground state $X^1\Sigma_g^+$. The strong OI 130.4 nm and 135.6 nm lines and several NI lines (120.0 nm, 122.8 nm, 124.3 nm, 131.1 nm, 131.9 nm, 132.7 nm, 141.2 nm, 149.3 nm, 174.4 nm) are also present.

[6] The FUV spectral response of TIMED/GUVI [*Paxton et al.*, 1999], IMAGE/FUV [*Mende et al.*, 2000], and the spectral response of the bandpasses used to derive the electron characteristics on POLAR/UVI [*Torr et al.*, 1995] are overplotted on the electron auroral spectrum in Figure 2. Brightness ratios and brightnesses are used in order to retrieve the electron incident mean energy and energy flux. Both POLAR/UVI and TIMED/GUVI use two spectral regions covering parts of the spectrum where $N_2$ LBH emissions are dominant and where the $O_2$ atmospheric absorption through dissociative excitation in the Schumann-Runge continuum (130–180 nm) is very different [e.g., *Germany et al.*, 1997; *Lummerzheim et al.*, 1997]. The "LBH short" (LBHs) channel, in the vicinity of 150 nm, is sensitive to emissions which experience extinction by Schumann-Runge bands of $O_2$, whereas the "LBH long" (LBHl) channel, in the vicinity of 170 nm, is sensitive to emissions which undergo little absorption by $O_2$, as illustrated in Figure 3. As a result, the brightness ratio between the two channels is a function of the $O_2$ density column at the altitude of the emission peak, that is, a function of the altitude of the emission peak. Using an electron transport model, a relation can be established between the altitude of the emission peak and the mean energy of the incident particles. For energies below 0.2 keV, the $O_2$ density column above the altitude of the emission peak is too low to cause significant extinction. This limits the method based

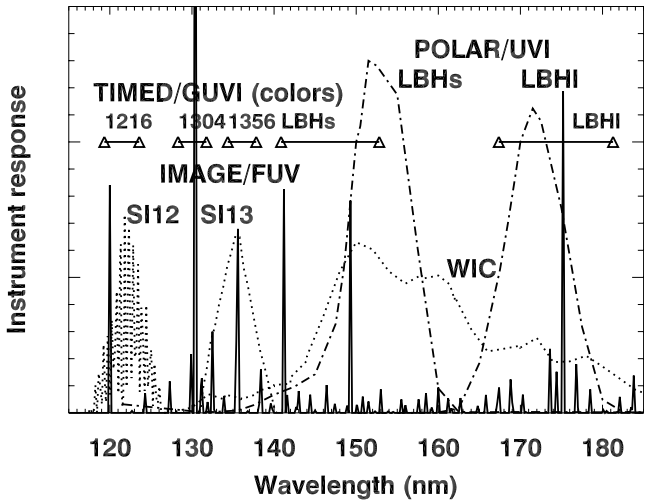


**Figure 2.** Response of the FUV instruments, including POLAR/UVI, for only the LBHs and LBHl channels (dashed-dotted lines), TIMED/GUVI (triangles), and IMAGE/FUV (dotted lines). The response is given in arbitrary units. The FUV spectrum presented in Figure 1 is overplotted as reference. For TIMED/GUVI, only the spectral coverage of the different channels is shown. The response of its LBH channels has a trapezoidal shape which is constructed from the spectrum obtained by a spectrometer with 1.8 nm resolution.

on LBH brightness ratio to retrieve the electron mean energy. As LBHl is sensitive to emissions not strongly absorbed in the atmosphere (as long as the mean energy of the incident electrons is less than about 15–20 keV), the LBHl brightness is less sensitive to the electron mean energy and can be scaled for inferring the energy flux of the incident electrons. For retrieving information on hard (>20 keV) electron precipitation, an X-ray imager, such as POLAR/Polar Ionospheric X-ray Imaging Experiment (PIXIE), sensitive to Bremsstrahlung from electrons of energies larger than 3 keV [e.g., *Anderson et al.*, 2000; *Østgaard et al.*, 2000; *Petrinec et al.*, 2000]. Unlike TIMED/GUVI and IMAGE/FUV, the images taken by POLAR/UVI in different spectral channels are not collected simultaneously. POLAR/UVI has to change filters between LBHs and LBHl exposures. If the aurora changes on time scales of less than one minute, this causes errors in the UVI data analysis.

[7] Instead of the LBHs and LBHl channels, IMAGE/FUV uses the Spectrographic Imager (SI)-13 around OI 135.6 nm and the Wideband Imaging Camera (WIC) covering the whole $N_2$ LBH range, as illustrated in Figure 2. The OI 135.6 nm is an emission more suitable than OI 130.4 nm to use for the analysis of the electron aurora, as it is not as strongly affected by resonance scattering as OI 130.4 nm is. Multiple scattering of OI 135.6 nm can be neglected for viewing angles close to nadir. For IMAGE, the electron characteristics are retrieved from the WIC to SI13 ratio and the WIC brightness [*Frey et al.*, 2002, 2003b]. Such an approach has the disadvantage to analyze brightnesses acquired by two kinds of instruments and dominated by emissions produced by different atmospheric components. The derivation of the electron mean energy is strongly dependent on the $N_2$ to O ratio, which is very sensitive to the magnetospheric activity [e.g., *Strickland et al.*, 1999; *Drob et al.*, 1999]. In addition, the retrieval of the energy flux is very sensitive to the electron mean energy, as the WIC spectral range covers part of the $N_2$ LBH emissions which is strongly affected by $O_2$ absorption.

## 3. Contribution of Proton Precipitation to FUV Brightnesses

### 3.1. Model Description

[8] The FUV spectra in electron and proton aurora are assessed from a comprehensive combined electron/proton kinetic model. The transport of incident energetic protons in the atmosphere is described by the multistream proton transport code developed by *Galand* [1996], which solves the steady-state Boltzmann equations for both protons and H atoms and are coupled through charge-changing reactions. This code has been successfully validated [*Galand et al.*, 1997] by comparison with rocket particle data [*Søraas et al.*, 1974] and by comparison with the model of *Basu et al.* [1993]. The transport of the energetic electrons is described by the multistream electron transport code developed by *Lummerzheim et al.* [1989], which solves the steady-state Boltzmann equation for electrons. The energetic electron population includes the electrons precipitating from the magnetosphere, the secondary electrons produced by ionization of electrons with the atmospheric species, and the secondary electrons produced within the proton beam by H or $H^+$ impact on the atmospheric species. The electron model was successfully validated by comparison with in situ particle measurements [*Lummerzheim et al.*, 1989] and by comparison with laboratory experiment [*Lummerzheim and Lilensten*, 1994]. The electron and proton transport codes are coupled through the source function of the secondary electrons produced inside the proton beam, which is an output of

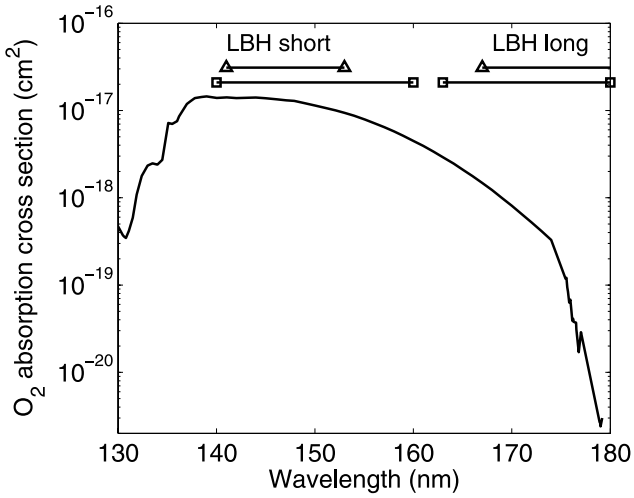


**Figure 3.** $O_2$ photoabsorption cross section over the Schumann-Runge continuum [*Ogawa and Ogawa*, 1975; *Starr*, 1976; *Gibson et al.*, 1983; *Lewis et al.*, 1985]. The spectral extents of the LBHs and LBHl channels for POLAR/UVI (squares) and TIMED/GUVI (triangles) have been added for reference.

the proton model and an input of the electron code [e.g., *Lummerzheim et al.*, 2001; *Galand et al.*, 2002].

[9] The incident electron and proton fluxes are assumed to be isotropic over the downward hemisphere and to have a Maxwellian distribution in energy. The energy flux is normalized to 1 mW $m^{-2}$. The mean energy of the incident particles ranges from 0.2 keV to 20 keV for electrons and from 5 keV to 25 keV for protons, typical values within the afternoon sector of the auroral oval studied in section 5. The neutral atmosphere ($N_2$, $O_2$, and O), adopted in both kinetic models, is specified by the Mass Spectrometer and Incoherent Scatter model (MSIS-90) [*Hedin*, 1991] for the location of Tromsø (69.58°N, 19.21°E), in the afternoon sector (1730 MLT), for a magnetic activity of $K_p = 4$, and a solar activity representative of average conditions ($F_{10.7} = 150 \cdot 10^{-22}$ $Wm^{-2}Hz^{-1}$). Note that the results presented in this section are affected by less than 5% when the neutral atmosphere is derived for a magnetic activity reduced down to $K_p = 2$. Therefore they can also be used for more magnetically quiet conditions. No field-aligned electric field is considered. It was checked that the mirroring effect of the magnetic field on the incident proton beam does not have any effect on the FUV brightnesses. The dip angle is 90°. The upper altitude is taken to be 600 km. It was checked that the FUV brightnesses are not affected if this altitude is increased. The collision cross section set used for proton and H atom impacts is described by *Lanchester et al.* [2003] and includes collisional angular redistribution below 1 keV. Note that this process does not affect significantly the integrated FUV brightnesses. For electrons, the cross section set used is from *Lummerzheim and Lilensten* [1994].

[10] From the computed particle ($e^-$, $H^+$, H) fluxes, the neutral densities, and the cross sections, it is possible to determine the excitation rate induced by particle impact on neutral species. As the $N_2$ LBH system is associated with an upper state which has a 0.14 ms lifetime, its quenching does not occur significantly above 100 km and the $N_2$ LBH emissions can be considered as prompt [*Vallance Jones*, 1974]. The emission cross section for $H^+$ and H impacts is from *Strickland et al.* [1993] and for electron impact is from *Ajello and Shemansky* [1985]. The branching ratio for the vibrational transition leading to the different vibrational levels is from *Ajello and Shemansky* [1985] for electrons. We apply the same value for protons and H atoms. This is a reasonable assumption provided the vibrational levels of $N_2(a)$ are populated in a similar way by H and $H^+$ impact as by electron impact (D. Strickland, personal communication, 2000). For $O^5S^0$ yielding the prompt OI 135.6 nm emission the excitation cross section by H atom impact and electron impact on atomic oxygen is taken from *Edgar et al.* [1975] and *Zipf and Erdman* [1985], respectively. Dissociative excitation of $O_2$ by electrons is also considered [*Ajello*, 1971], but it is a less significant process compared to the direct excitation of O. The $O^5S^0$ excitation rate by proton impact is not considered, as it should be insignificant due to the nature of the transition [*Strickland et al.*, 1993]. The cross sections and branching ratios for the NI emissions are given by *Ajello and Shemansky* [1985].

[11] The computation of the brightness, or vertical column-integrated emission rate, requires one to take into account the strong $O_2$ photoabsorption. Photoabsorption cross sections by $O_2$ are taken from *Mohan* [1979], *Ogawa and Ogawa* [1975], *Starr* [1976], *Gibson et al.* [1983], and *Lewis et al.* [1985] (see Figure 3). Note that all the FUV brightnesses presented in Figures 4, 5, 6, and 7 are shown with solid lines for electron precipitation and dashed lines for proton precipitation. The latter includes the contribution

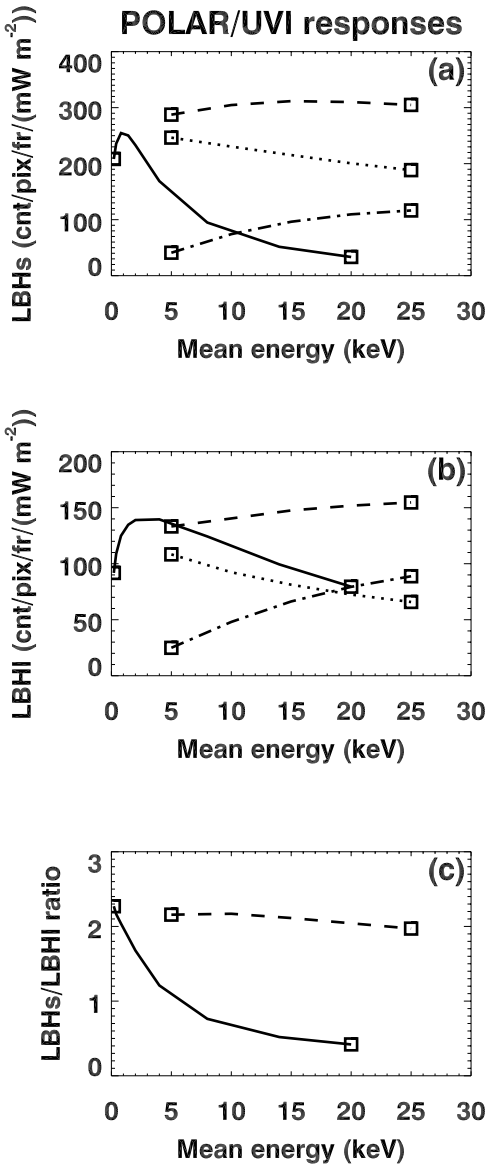


**Figure 4.** Results for incident electron (solid line) and proton (dashed line) fluxes with a Maxwellian distribution in energy and a normalized energy flux of 1 mW $m^{-2}$. The results are presented as a function of the mean energy of the particles, that is, two times the peak energy, as Maxwellian distributions are assumed. The proton contribution is separated in two components, that associated with direct impacts by $H^+$ and H (dotted line) and that associated with impacts from secondary electrons produced within the proton beam (dashed-dotted line). (a) Response of the FUV channel covering a part of the spectrum strongly affected by $O_2$ absorption (LBHs), (b) response to the FUV channel used for retrieving the energy flux (LBHl), and (c) LBHs to LBHl response ratio used for retrieving the electron mean energy.

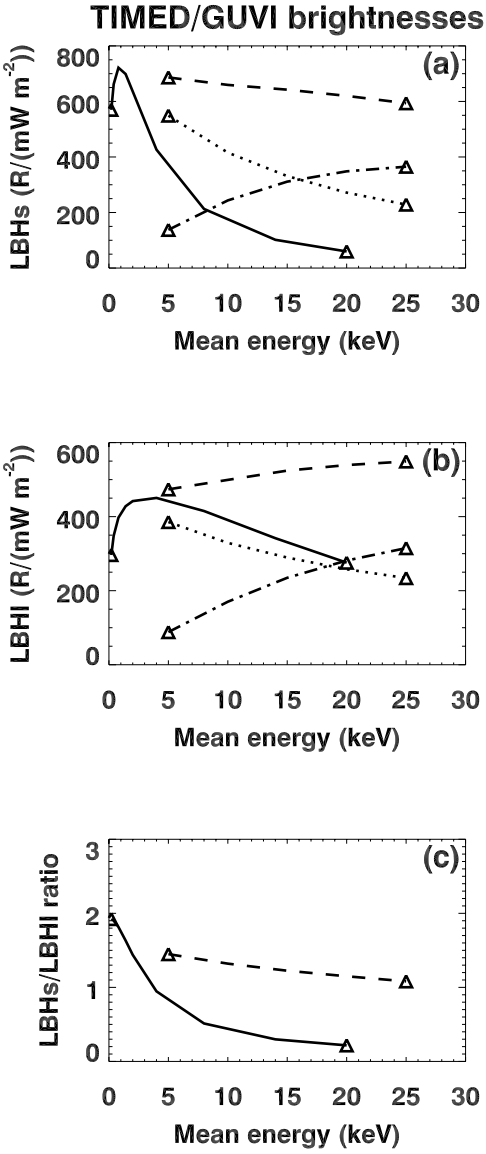


**Figure 5.** Same as Figure 4 but for TIMED/GUVI. (a) LBHs brightness, (b) LBHl brightness, and (c) LBHs to LBHl brightness ratio.

by direct impact of protons and H atoms (dotted lines) and by secondary electrons (dashed-dotted lines). The POLAR/UVI, TIMED/GUVI, and IMAGE/FUV responses are shown with squares, triangles, and crosses, respectively.

### 3.2. FUV Brightnesses in Electron and Proton Aurora

[12] Figures 4a and 4b show the brightness response of the POLAR/UVI filters. In electron aurora (solid lines) the brightness is sensitive to the mean energy of the incident particles. As the mean energy increases, the electrons penetrate deeper into the atmosphere and the FUV-induced emissions undergo a larger extinction by $O_2$ bands, especially for the LBHs channel (see Figure 3). As a result, the LBHs to LBHl ratio is strongly dependent on the electron mean energy and is thus suitable for retrieving it (see Figure 4c). In proton aurora (dashed lines), the brightnesses are less sensitive to the mean energy of the incident particles, confirming earlier findings [*Strickland et al.*, 1993; *Galand et al.*, 2002]. The decrease in brightness of the emission induced by $H^+$/H impact is compensated by the increase of the secondary electron contribution and oxygen molecule absorption is a rather secondary effect in proton aurora. Similar results are obtained with TIMED/GUVI (see Figures 5). For LBHs the $O_2$ attenuation experienced by GUVI is larger than that associated with POLAR/UVI. The GUVI/LBHs channel extends less towards high wavelengths than the UVI/LBHs, as illustrated in Figure 3. Furthermore, the GUVI/LBHl channel is covering a domain which is less affected overall by $O_2$ absorption than UVI/LBHl. Assuming an emission ratio similar between POLAR/UVI and TIMED/GUVI, the LBHs to LBHl ratio is expected to be smaller for TIMED/GUVI than for POLAR/UVI. This is clearly seen in proton aurora. High-energy protons look to these instruments like low-energy electrons, with a brightness ratio similar to electrons of energies lower than 1 keV for

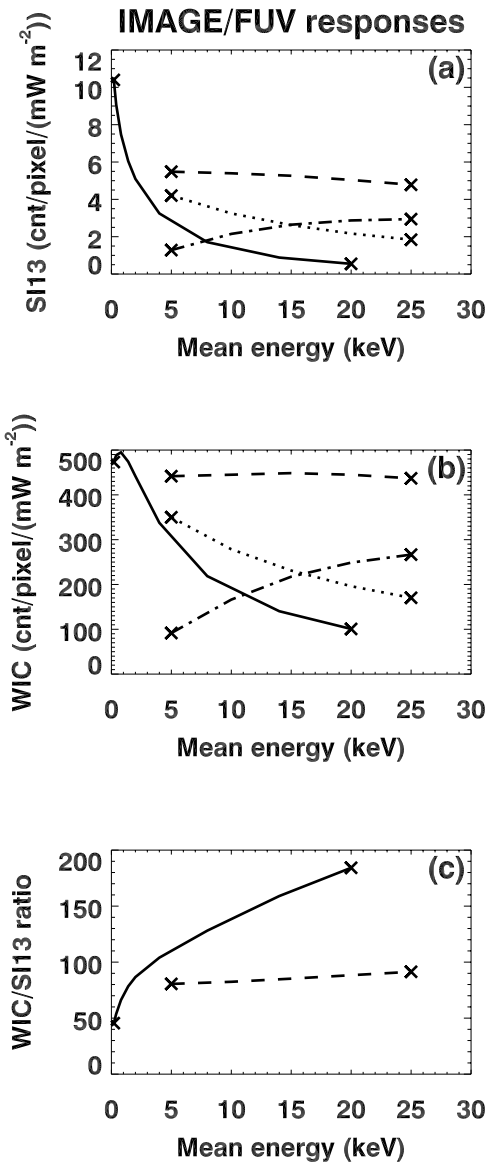


**Figure 6.** Same as Figure 4 but for IMAGE/FUV. (a) SI13 response, (b) WIC response, and (c) WIC to SI13 ratio.

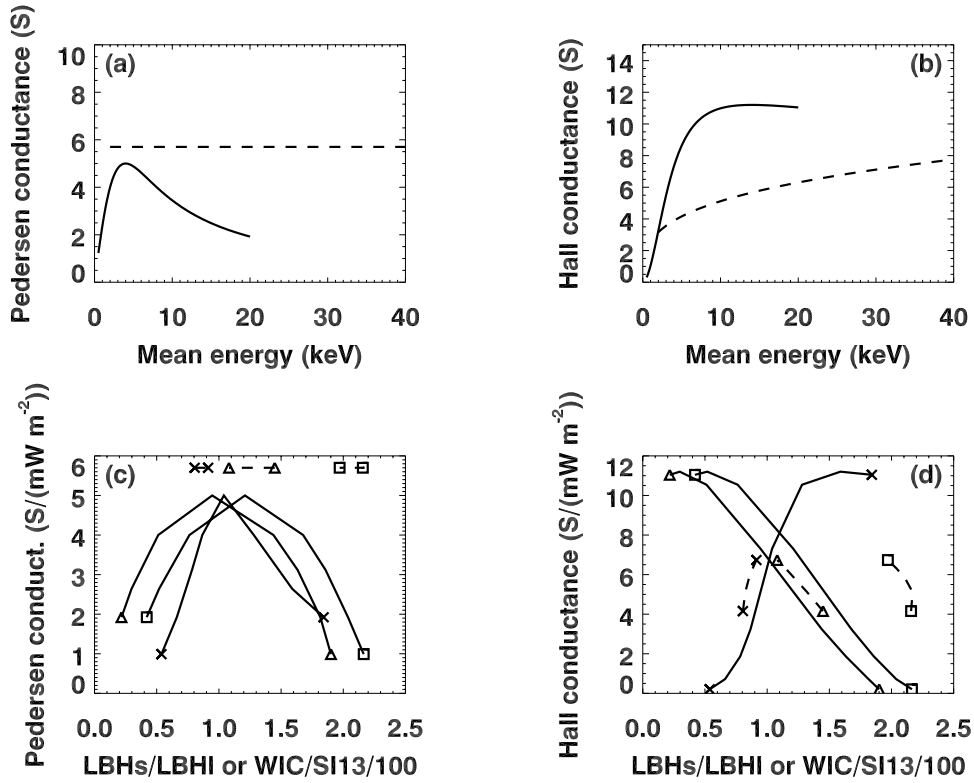


**Figure 7.** (a) Pedersen conductance as a function of the electron (solid line) and proton (dashed line) mean energy. The parametrization is from *Robinson et al.* [1987] for electrons and from *Galand and Richmond* [2001] for protons. The incident energy flux is 1 mW $m^{-2}$ and the incident particle flux is assumed to be Maxwellian. (b) Same as Figure 7a, except for Hall conductance. (c) Pedersen conductance caused by electrons (solid line) and protons (dashed line) as a function of the FUV brightness ratio used to infer the electron mean energy. The particle mean energy is varied along each line from 0.4 keV to 20 keV for electrons and from 5 keV to 25 keV for protons. The incident energy flux is 1 mW $m^{-2}$ and the incident particle flux is assumed to be Maxwellian. The results for POLAR/UVI, TIMED/GUVI, and IMAGE/FUV are presented with square, triangle, and cross symbols, respectively. This plot is based on results presented in Figures 7a, 4c, 5c, and 6c. (d) Same as Figure 7c but for Hall conductance.

POLAR/UVI (see Figure 4c) and of energies in the 2.0–3.5 keV range for TIMED/GUVI (see Figure 5c).

[13] For IMAGE/FUV, in electron aurora the SI13 and WIC channel responses strongly decrease with energy in electron aurora due to $O_2$ absorption (see Figures 6a and 6b, solid lines). In proton aurora, these channels are sensitive at low energies (<15 keV) to direct H impact on atomic oxygen (dotted lines) and at higher energies to excitation by secondary electrons produced in the proton beam (dashed-dotted lines). As a result, the SI13 and WIC responses are fairly independent of the mean energy of the incident protons. In the case of IMAGE/FUV, protons look like electrons of energies in the 1.5–2.5 keV range (see Figures 6b and 6c). The results presented in Figure 6 are in good agreement with those obtained by *Frey et al.* [2003b]. The small discrepancies found can be explained by the difference in the neutral atmosphere model. For protons, the different distributions assumed for the incident beam (Maxwellian versus Kappa-law) also account for the discrepancies.

[14] For the three sets of instruments, POLAR/UVI, TIMED/GUVI, and IMAGE/FUV, protons in the keV range produce a similar response in the FUV channels as low energy electrons. Without knowledge of the type of precipitation, the interpretation of FUV brightness and brightness ratios in terms of energy and energy flux of the preciptiating auroral particles can therefore give errors. Assuming that all observed auroral brightness is caused by electron precipitation yields an underestimation of the electron mean energy in regions of >4 keV electron precipitation. The underestimation is observed for POLAR/UVI down to energies as low as 1 keV. The FUV brightnesses in proton aurora, which are used to derive the particle energy flux, are not strongly dependent on the particle mean energy. They have values similar to those produced by low-energy electrons, assuming the same incident energy flux (see Figures 4b, 5b, and 6b). Therefore in regions of low-energy (<4 keV) electron precipitation or in regions dominated by proton precipitation, the estimation of the energy flux from FUV brightnesses assuming pure electron precipitation is expected to be fairly insensitive to the presence of proton precipitation.

## 4. Estimation of Ionospheric Conductances

[15] The response of FUV instruments on board POLAR, TIMED, and IMAGE to proton precipitation is very similar to that of few keV electrons, as presented in section 3.2. Energetic protons are more efficient to ionize than low-

energy electrons [e.g., *Galand et al.*, 1999] and cause different ionospheric conductances. It is thus important to estimate how significant the misinterpretation of the auroral emissions is in the presence of proton precipitation when these derivations are based on brightnesses and brightness ratios that assume pure electron precipitation.

[16] In order to assess the perpendicular electrical ionospheric conductances, we use the parameterizations given by *Robinson et al.* [1987] for electrons and by *Galand and Richmond* [2001] for protons. These simplified relations provide the ionospheric conductances induced by particle precipitation, given the mean energy and energy flux of the incident beam. They were developed for incident fluxes assumed to be Maxwellian in energy, like in our simulations. The dependence of the Pedersen ($\Sigma_P$) and Hall ($\Sigma_H$) conductances in mean energy is illustrated in Figures 7a and 7b, respectively, for an incident energy flux of 1 mW m$^{-2}$. It is very different for keV protons (dashed lines) and electrons (solid lines), as explained by *Galand and Richmond* [2001].

[17] For protons, the dependence in energy of the Pedersen conductance is fairly weak with a value for $\Sigma_P$ close to 5.7 S, whereas for electrons the Pedersen conductance is strongly dependent on the mean energy with a maximum reached at 4 keV with a value of 5 S (for an incident energy flux of 1 mW m$^{-2}$), as illustrated in Figure 7a. Therefore the misinterpretation of the particle mean energy has no effect on the assessement of $\Sigma_P$ in proton-dominated aurora, whereas it can lead to a poor estimation of $\Sigma_P$ in electron-dominated aurora (assuming a good estimation of the particle energy flux). $\Sigma_P$ has always larger values in proton aurora than in electron aurora for a given energy flux. Therefore in proton-dominated aurora, whatever the value estimated for the mean energy, $\Sigma_P$ is always underestimated when its value is derived from FUV brightnesses assuming pure electron precipitation. This underestimation is greater than 12% in regions of pure proton aurora. This is valid under the condition that the particle energy flux has been well assessed.

[18] Figure 7b is similar to Figure 7a but for the Hall conductance. $\Sigma_H$ induced by electron precipitation has a strong dependence on energy with a sharp decrease with decreasing mean energy below 8 keV and has a value close to 11 S for larger mean energies. A misinterpretation of the electron mean energy yields a very poor estimation of the Hall conductance. In proton aurora, $\Sigma_H$ increases with mean energy but over a smaller range of values than in electron aurora. The misinterpretation of the mean energy has much less influence on the estimation of the Hall conductance in proton aurora than in electron aurora, when the value of $\Sigma_H$ is retrieved from FUV brightnesses assuming the correct particle type.

[19] A given value of the particle mean energy corresponds to a value for $\Sigma_P$ (cf. Figure 7a), a value for $\Sigma_H$ (cf. Figure 7b), and a value for the FUV brightness ratio (cf. Figures 4c, 5c, and 6c), if we know the incident energy flux. Figures 7c and 7d show $\Sigma_P$ and $\Sigma_H$, respectively, as a function of the FUV brightness ratio, when the particle mean energy is varied from 0.4 keV to 20 keV for electrons (solid lines) and from 5 keV to 25 keV for protons (dashed lines). The incident energy flux for all cases is 1 mW m$^{-2}$. Assuming that the FUV brightness gives a good estimate of the particle energy flux, the brightness ratios used to derive the particle mean energy, and thus the electrical conductances, result in underestimated $\Sigma_P$ and $\Sigma_H$ in proton-dominated aurora. For instance, in Figure 7c, for an incident energy flux of 1 mW m$^{-2}$, a brightness ratio of 2 obtained with POLAR/UVI provides a value for the Pedersen conductance of 2.2 S in pure electron precipitation and of 5.7 S in pure proton precipitation. Therefore if pure electron precipitation is assumed for the analysis in a region of pure proton precipitation, the Pedersen conductance is underestimated by 61% for a brightness ratio of 2 obtained from POLAR/UVI. Overall, the discrepancy is significant for POLAR/UVI, with an underestimation of at least 60% for $\Sigma_P$ and 85% for $\Sigma_H$ in pure proton precipitation. For TIMED/GUVI the underestimation is larger than 18% for $\Sigma_P$ and 15% for $\Sigma_H$. For IMAGE/FUV the underestimation is larger than 23% for $\Sigma_P$ and 33% for $\Sigma_H$.

[20] In section 3.2 it was found that in proton-dominated aurora the estimation of the energy flux from FUV brightnesses assuming pure electron precipitation is fairly good. The brightness in LBHl and WIC channels in proton aurora has values close to those produced by electrons of energy similar to the energy of the electrons which have the same brightness ratio signature as protons. As a consequence, it is expected that the electrical conductances assessed from FUV brightnesses and brightness ratios assuming pure electron precipitation are underestimated when proton precipitation is the dominant particle input.

## 5. Retrieving Physical Quantities in the Afternoon Sector

[21] The previous section discussed the errors in the analysis of FUV brightness for hypothetical mixtures of electron and proton aurora where both types of precipitation carried the same energy flux. In order to estimate the errors in realistic aurora situations, we perform a numerical experiment driven by average auroral inputs. We use the combined electron and proton auroral model to obtain FUV brightnesses, calculate the response of various instruments, and finally take these ''measurements'' and interpret them under the assumption that only electron aurora was present.

[22] The misinterpretation of the FUV brightnesses for retrieving the electron mean energy, the total (electron plus proton) energy flux, and the particle-induced ionospheric conductances is assessed in the afternoon sector of the equatorial edge of the auroral oval, where protons are a dominant particle energy input over the ionosphere [e.g., *Hardy et al.*, 1989; *Galand et al.*, 2001]. The energy flux and mean energy of the incident electrons and protons are obtained from the Air Force Research Laboratory's auroral statistical model derived from the polar-orbiting Defense Meteorological Satellite Program (DMSP) particle data [*Hardy et al.*, 1987; *Hardy et al.*, 1989]. The electron characteristics are derived as explained by *Galand et al.* [2001]. The extrapolation towards high energies for both particle types is based on a Maxwellian distribution, which is the distribution used to define the incident particle flux in our simulations. We extract the electron and proton mean energy (Figure 8a) and energy flux (Figure 8b) for a magnetic activity of $K_p = 4$ and for the location of Tromsø, Norway (66.4°N geomagnetic latitude).

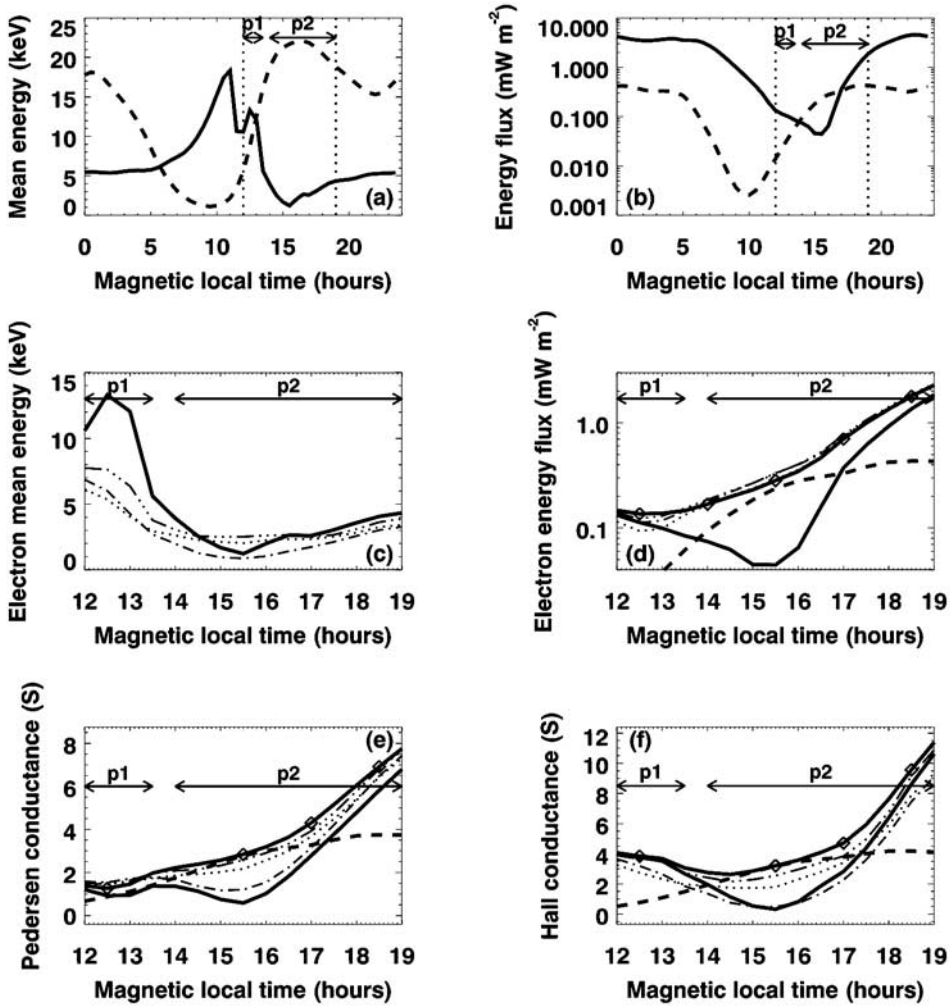


**Figure 8.** Application to the location of Tromsø, Norway (66.4° magnetic latitude), for a magnetic activity of $K_p$ = 4. The region of study is divided in two: period 1, marked "p1" on the plots, corresponding to precipitation dominated by >4 keV electrons with the presence of a proton component, and period 2, marked "p2" on the plots, corresponding to precipitation dominated by protons (until 1700 UT) in presence of a soft electron component. The thick lines correspond to the variables derived from the DMSP statistical patterns. The thin lines are associated with the FUV instruments. (a) Electron (solid line) and proton (dashed line) mean energy as a function of the magnetic local time. The data are from the statistical patterns derived from DMSP particle observations by *Hardy et al.* [1987] for electrons and *Hardy et al.* [1989] for protons (as explained by *Galand et al.* [2001]). The vertical dotted lines define the period of focus here. (b) Same as Figure 8a but for the particle energy flux. (c) Electron mean energy derived from the analysis of the FUV brightness ratios, assuming pure electron precipitation, for POLAR/UVI (dashed-dotted line), TIMED/GUVI (dashed-three-dotted line), and IMAGE/FUV (dotted line). The FUV brightnesses are computed from the particle characteristics presented in Figures 8a and 8b, using the results from Figures 4, 5, and 6. The electron mean energy from the statistical pattern is overplotted for reference (solid line). (d) Same as Figure 8c but for the particle energy flux. The estimated energy fluxes are derived from the LBHl channel for POLAR/UVI and TIMED/GUVI and from the WIC channel for IMAGE/FUV. The solid line with diamond represents the sum of the electron (solid line) and proton (dashed line) energy fluxes. (e) Pedersen conductance derived from the estimated electron characteristics presented in Figures 8c and 8d, for POLAR/UVI (dashed-dotted line), TIMED/GUVI (dashed-three-dotted line), and IMAGE/FUV (dotted line). The Pedersen conductance assessed using the particle characteristics from the statistical patterns plotted in Figures 8a and 8b is shown as solid line for electron precipitation, as dashed line for proton precipitation, and as solid line with diamond for the mixture of electrons and protons. The ionospheric conductances are computed applying the simple relations developed by *Robinson et al.* [1985] for electrons and by *Galand and Richmond* [2001] for protons. (f) Same as Figure 8e but for Hall conductance.

**Table 1.** Largest Errors Obtained Over Period 1 at the Location of Tromsø, Norway (66.4° Magnetic Latitude) for $K_p = 4$[a]

| Trend Obtained on the Estimated Physical Quantities | POLAR/UVI | TIMED/GUVI | IMAGE/FUV |
|---|---|---|---|
| Underestimation of the electron mean energy (see Figure 8c) | 65% | 47% | 66% |
| Underestimation of the particle energy flux (see Figure 8d) | 18% | 10% | 31% |
| Overestimation of the Pedersen conductance (see Figure 8e) | 21% | 13% | 15% |
| Underestimation of the Hall conductance (see Figure 8f) | 40% | 11% | 36% |

[a]Period 1, covering the 1200–1330 MLT period in Figures 8a–8b, corresponds to a time of precipitation dominated by >4 keV electrons with the presence of a proton component.

[23] We focus on the time period between 1200 and 1900 MLT (magnetic local time). Over this time period, protons carry a fair amount of energy flux upon the ionosphere. This period can be separated in two. Between 1200 and 1330 MLT, hereafter referred as "period 1," the precipitation is dominated by >4 keV electrons with a proton component. Between 1400 and 1900 MLT, hereafter referred as "period 2," the precipitation is dominated by energetic protons (until 1700 UT) with a soft electron component.

### 5.1. In > 4 KeV Electron-Dominated Aurora

[24] This section focuses on period 1, dominated by medium to hard electron precipitations with presence of a proton component. The electrons carry more than half of the total particle energy flux and their mean energy has values larger than 4 keV as attested by Figures 8a and 8b. Using the particle characteristics shown in Figures 8a and 8b, the FUV brightnesses, expected for POLAR/UVI, TIMED/GUVI, and IMAGE/FUV, are derived from the instrument responses illustrated in Figures 4, 5, and 6. The total FUV brightness for each instrument and channel is the sum of the brightness computed for electron precipitation and the brightness computed for proton precipitation. Using these total brightnesses, we estimate the particle mean energy from Figures 4c, 5c, and 6c and particle energy flux from Figures 4b, 5b, and 6b, assuming all particles to be electrons. The mean energy and energy flux derived for POLAR/UVI (dashed-dotted lines), TIMED/GUVI (dashed-three-dotted lines), and IMAGE/FUV (dotted lines) are shown in Figures 8c and 8d, respectively. The electron mean energy provided by the DMSP statistical model is also plotted as a solid line in Figure 8c as reference. The total energy flux, sum of both DMSP electron (solid lines) and proton (dashed lines) energy fluxes, is shown with diamonds in Figure 8d. An overview of the error on the different physical quantities retrieved from the FUV brightnesses and brightness ratios is given in Table 1.

[25] The presence of protons in a region of >4 keV electron precipitation results in a large underestimation of the electron mean energy (cf. Figure 8c and Table 1). The brightness ratios used for retrieving the mean energy have values in proton aurora similar to those corresponding to electron mean energies lower than the actual energy of the precipitating electron population (see Figures 4c, 5c, and 6c). The underestimation of the electron mean energy with values above 4 keV yields an underestimation of the particle energy flux (see Figure 8d and Table 1), as predicted by Figures 4b, 5b, and 6b. For IMAGE/FUV, even though protons carry only 10% of the energy flux at 1200 MLT, the particle energy flux is underestimated by 31% at that time. For POLAR/UVI and TIMED/GUVI, the poor estimation of the energy flux is not as significant (see Table 1), as the LBHl channels used to retrieve the energy flux have a response less dependent on the electron mean energy than the WIC channel.

[26] To calculate the perpendicular electrical ionospheric conductances (see Figures 7a and 7b) we use the same procedure as described in section 4. The Pedersen and Hall conductances derived from the DMSP particle characteristics (see Figures 8a and 8b) are shown with solid line for electrons and dashed line for protons in Figures 8e and 8f, respectively. The total Pedersen and Hall conductances are shown with diamonds in Figures 8e and 8f. The conductances are also estimated from the particle mean energy and energy flux derived using the FUV brightnesses and brightness ratios assuming pure electron precipitation. The Pedersen and Hall conductances are plotted as dashed-dotted line for POLAR/UVI, dashed-three-dotted line for TIMED/GUVI, and dotted line for IMAGE/FUV in Figures 8e and 8f, respectively.

[27] The estimated electron mean energy over period 1 is larger than 4 keV (see Figure 8c), the value corresponding to the maximum in the Pedersen conductance (see Figure 7a). Therefore the underestimation of the electron mean energy compensates the underestimation of the energy flux (see Figure 8d) and the presence of proton precipitation yields an overestimation of the Pedersen conductance (see Figure 8e and Table 1).

[28] Over period 1 the incident electrons have large enough energies to provide Hall conductance of values greater than those induced by protons for a given particle energy flux. However, the Hall conductance induced by electron precipitation decreases sharply with decreasing mean energy below 8 keV, as shown in Figure 7b. The underestimation of both the electron mean energy and energy flux induced by the presence of proton precipitation yields an underestimation of the Hall conductance (see Figure 8f and Table 1).

### 5.2. In Proton-Dominated Aurora With a Soft Electron Component

[29] This section focuses on period 2 (1400–1900 MLT), dominated by proton precipitation until 1700 UT with a soft electron component over the whole period. The electron mean energy is primarily smaller than 4 keV (see Figure 8a). Protons carry most of the particle energy input until 1700 UT, up to 84%. This percentage is reached for an energy flux of 0.24 mW $m^{-2}$ (see Figure 8b). The maximum value for the proton energy flux over period 2 is 0.43 mW $m^{-2}$. The derivation of the results presented in Figures 8c–8f are explained in details in section 5.1. An overview of the error on the different physical quantities retrieved from the FUV brightnesses and brightness ratios is given in Table 2.

[30] Over the whole period 2 the electron mean energy derived from POLAR/UVI channels is always underesti-

**Table 2.** Largest Errors Obtained Over Period 2 at the Location of Tromsø, Norway (66.4° Magnetic Latitude) for $K_p = 4$[a]

| Trend Obtained on the Estimated Physical Quantities | POLAR/UVI | TIMED/GUVI | IMAGE/FUV |
|---|---|---|---|
| Underestimation of the electron mean energy (see Figure 8c) | 50% | 22% | 33% |
| Overestimation of the electron mean energy between ~1430 and ~1630 UT (see Figure 8c) | −50% | 106% | 67% |
| Estimation of the particle energy flux (see Figure 8d) | 18% | 16% | 4% |
| Underestimation of the Pedersen conductance (see Figure 8e) | 58% | 10% | 23% |
| Underestimation of the Hall conductance (see Figure 8f) | 85% | 21% | 44% |

[a]Period 2, covering the 1400–1900 MLT period in Figure 8a–8b corresponds to a time of precipitation dominated by protons (until 1700 UT) with the presence of soft (<4 keV) electrons.

mated (cf. Figure 8c and Table 2). The protons produce an FUV brightness like electrons of energies always smaller than the energy of the actual incident electrons (less than 1 keV, as illustrated in Figure 4c). For TIMED/GUVI and IMAGE/FUV, protons look as if they were electrons between 2.0 and 3.5 keV (see Figure 5c) and between 1.5 and 2.5 keV (see Figure 6c), respectively. The electron mean energy obtained from the ratio of the total brightnesses (see Figure 8c) is underestimated when the energy of the incident electrons is larger than the actual energy and is overestimated when it is smaller than the actual energy in these ranges. Owing to the presence of a low-energy electron precipitation, the electron mean energy is largely overestimated over period 2 for TIMED/GUVI and IMAGE/FUV (see Figure 8c and Table 2).

[31] In this region of mixture of precipitating protons and low-energy electrons, the poor estimation of the electron mean energy has only minor impact on the determination of the particle energy flux (see Figure 8d). The response of the LBHl and WIC channels to protons is similar to the response to 1–3 keV electrons, which have the same brightness ratio signature as protons (see Figures 4, 5, and 6). The estimation of the particle energy flux is fairly good, by less than 18%, as shown in Table 2.

[32] During period 2 the DMSP electron mean energy is less than 4 keV (see Figure 8a). When the mean energy is underestimated (see Figure 8c), the sharp decrease of the electron-induced Pedersen conductance with decreasing mean energies (see Figure 7a) causes a large underestimation of the Pedersen conductance (see Figure 8e). The largest underestimation is found for POLAR/UVI for which the estimated mean energy has the lowest values, as given in Table 2. Even when the mean energy is overestimated, the larger values obtained for the Pedersen conductances assuming pure electron precipitation cannot completely compensate the presence of proton precipitation, which are the dominant energy source and which are more efficient to ionize than low-energy electrons. Over period 2 the DMSP electron mean energy is less than 8 keV, below which the Hall conductance decreases sharply with decreasing mean energy (see Figure 7b). Therefore the underestimation of the electron mean energy yields a large underestimation of the Hall conductances (see Figure 8f). This is particularly true for POLAR/UVI, as shown in Table 2. Even when the electron mean energy is overestimated, energetic protons are more efficient to produce Hall conductance than the estimated mean energy electrons.

[33] Although this analysis is specific for the location of Tromsø, the results are not unique. We carried out a similar numerical experiment for the location of Poker Flat with similar results illustrated in Table 3. Poker Flat (65.2°N magnetic latitude) also passes underneath the afternoon sector of the equatorial region of the auroral oval. Over this location, for $K_p = 4$, between 1200 and 1900 MLT protons carry up to 94% of the particle energy input with an energy flux of 0.22 mW $m^{-2}$. The maximum in proton energy flux is reached at 1900 MLT with a value of 0.55 mW $m^{-2}$. The electron mean energy is less than 7 keV in the 1200–1900 MLT period. As a result, the behavior found at Poker Flat is very similar to that found at Tromsø with a weaker period 1-type region and a stronger period 2-type region.

[34] In the period around midnight, protons are not a dominant energy source, carrying less than 20% of the total energy flux above Tromsø for $K_p = 4$, and the electron population is not too hard with energies around 5 keV. Under such conditions, the influence of protons on the estimation of the electron energy flux and mean energy and of the Pedersen and Hall conductances is more modest, as illustrated in Table 4. The use of brightnesses and brightness ratios assuming pure electron precipitation is thus a suitable approach to retrieve electron characteristics and ionospheric conductances.

## 6. Discussion

[35] Proton precipitation contributes significantly to the FUV emissions used for retrieving the electron mean energy and energy flux. In regions where proton precipitation is significant or in regions of >4 keV electron precipitation with additional proton precipitation, caution should be applied to the determination of electron characteristics and ionospheric conductances. Large errors can result when

**Table 3.** Largest Errors Obtained Over the 1200–1900 MLT Period at the Location of Poker Flat, Alaska (65.2° Magnetic Latitude) for $K_p = 4$[a]

| Trend obtained on the estimated physical quantities | POLAR/UVI | TIMED/GUVI | IMAGE/FUV |
|---|---|---|---|
| Underestimation of the electron mean energy | 60% | 30% | 43% |
| Overestimation of the electron mean energy between 1430 and 1700 MLT | −60% | 145% | 97% |
| Estimation of the energy flux | 19% | 19% | 15% |
| Underestimation of the Pedersen conductance | 59% | 11% | 22% |
| Underestimation of the Hall conductance | 86% | 19% | 40% |

[a]This period is characterized by precipitation of <7 keV electrons with presence of protons.

**Table 4.** Largest Errors Obtained Over the 1900–0400 MLT Period at the Location of Tromsø, Norway (66.5° Magnetic Latitude) for $K_p = 4$

| Trend Obtained on the Estimated Physical Quantities | POLAR/UVI | TIMED/GUVI | IMAGE/FUV |
|---|---|---|---|
| Underestimation of the electron mean energy | 25% | 11% | 26% |
| Estimation of the energy flux | 3% | 1% | 10% |
| Estimation of the Pedersen conductance | 3% | 1% | 6% |
| Underestimation of the Hall conductance | 20% | 4% | 20% |

conductances are derived from FUV brightnesses and brightness ratios assuming pure electron precipitation, such as from POLAR/UVI, TIMED/GUVI, IMAGE/FUV, as well as from the Defense Meteorological Satellite Program (DMSP)/Special Sensor Ultraviolet Spectrographic Imager (SSUSI) [*Paxton et al.*, 2002] launched in October 2003.

[36] The FUV instrument responses and brightness ratios in proton aurora are less sensitive to the mean energy of the incident particles than in electron aurora. The reason is threefold. The keV protons deposit their energy above 110 km where the $O_2$ absorption is not too strong. The altitude range of the emission peak is relatively small over the 5–25 keV energy range, compared with the altitude range of auroral electrons. The contribution of secondary electrons increases with the proton mean energy, compensating the brightness decrease in energy of the emission produced by direct $H^+$/H impact. Energetic protons in the keV range produce the same FUV signatures as electrons of low energy.

[37] In particular, the FUV brightness ratios from protons of 5–25 keV, which are used for retrieving the electron mean energy, have the same signature as electrons of energies less than 1 keV for POLAR/UVI, between 2.0 and 3.5 keV for TIMED/GUVI, and between 1.5 and 2.5 keV for IMAGE/FUV. Therefore when precipitating electrons have energies outside these ranges, the presence of proton precipitation yields a large misinterpretation of the electron mean energy. In presence of >4 keV electron precipitation, such as in the early afternoon sector of the equatorial edge of the auroral oval, the presence of protons, even with a small energy flux and far from being the dominant precipitation, yields a large underestimation of the electron mean energy. As the response of the FUV channels used for retrieving the particle energy flux is similar between protons over the whole keV range and electrons of low energies, the derivation of the total energy flux is relatively good in proton-dominated aurora, such as the afternoon sector of the equatorial edge of the auroral oval. It is, however, overestimated in regions of mixture of >4 keV electrons and keV protons, such as in the early afternoon sector of the equator edge of the auroral oval. Assuming a good estimation of the particle energy flux, the underestimation of the electron mean energy yields an overestimation of the Pedersen conductance, when the estimated mean energy is larger than 4 keV, and an underestimation of the Pedersen conductance, when the precipitating electrons have energies lower than 4 keV. Regarding the Hall conductance, it is found that it is always underestimated in the equatorial edge of the afternoon auroral oval. The estimation of the Pedersen and Hall conductances is very poor (>∼60%) for POLAR/UVI in regions of dominant proton precipitation, as protons which do ionize look like very low-energy electrons, which do not contribute significantly to the ionospheric conductances.

[38] The contribution of the proton precipitation to the FUV brightnesses is largely dominated by the estimation of the $N_2$ LBH emission induced primarily by $H^+$ and H impacts for mean energy below 15 keV. Unfortunately, the only $N_2$ LBH emission cross section for H impact available to our knowledge is from a crude estimate [*Strickland et al.*, 1993]. In addition, owing to a lack of measurements, the $N_2$ LBH branching ratios in proton aurora are assumed to be equal to the ones for electrons. Laboratory measurements and in situ multi-instrument experiments are drastically needed to improve our ability to assess the $N_2$ LBH emission in proton aurora.

[39] As a consequence of the contribution of protons to the FUV brightnesses used for retrieving the conductances, the proton component of the precipitation should be assessed separately. Proton aurora can be distinguished from electron aurora by the presence of hydrogen emissions. The abundance of ambient hydrogen in the thermosphere is too low to cause significant hydrogen emissions by electron precipitation. In proton aurora the excitation of the hydrogen atoms produced within the proton beam leads to Doppler-shifted hydrogen emissions. $H_\alpha$ and $H_\beta$ brightnesses observed from the ground have been used to infer qualitative information on the location of proton precipitation [e.g., *Donovan et al.*, 2003, *Deehr and Lummerzheim*, 2001], and the line profiles can be interpreted in terms of mean energy and energy flux of the precipitating protons [*Sigernes*, 1996; *Lorentzen et al.*, 1998; *Lummerzheim and Galand*, 2001; *Lanchester et al.*, 2003]. From space, the Visible Imaging System (VIS) instrument on POLAR observes the $H_\alpha$ emission, but it has not been able to successfully provide global imaging of the proton aurora due to the low brightness of this emission (J. Sigwarth, private communication, 1998). The H Lyman $\alpha$ line is much brighter than the visible Balmer lines and is usually used to track proton aurora from space [e.g., *Paresce et al.*, 1983; *Ishimoto et al.*, 1989; *Bertaux et al.*, 1984; *Strickland et al.*, 2001; *Galand et al.*, 2002]. Unlike POLAR, which does not have any capability to estimate the contribution from proton precipitation, IMAGE and TIMED do have a H Lyman $\alpha$ channel for a potential estimation of the proton contribution. The spectrographic imager SI-12 on IMAGE has been designed to focus on the Doppler-shifted H Lyman $\alpha$ by using spectral filtering to remove the geocoronal background. It has provided unprecedented images of the entire proton auroral oval from which qualitative information on the proton precipitation can be inferred [e.g., *Mende et al.*, 2001; *Frey et al.*, 2002, 2003a]. This channel can also be used for a potential correction of the proton contamination of the auroral images used for retrieving the electron characteristics, as illustrated by *Frey et al.* [2001] and explained by *Frey et al.* [2003b]. However, the data suffer contamination from the nearby NI 120.0 nm auroral emission and no information on the spectral shape of the

H Lyman $\alpha$ emission is given, which imposes strong limitations to any quantitative analysis. TIMED/GUVI has a H Lyman $\alpha$ channel which is sensitive to proton aurora [*Paxton et al.*, 1999]. In its routine mode, TIMED/GUVI also does not provide any spectral information over the bandpass of its different channels. At occasions this instrument is running in a spectrographic mode, which provides spectra of 1 nm resolution. Under such conditions, quantitative analysis is limited by stringent assumptions on the energy distribution of the incident particles [e.g., *Immel et al.*, 2002; *Strickland et al.*, 2001; *Galand et al.*, 2002]. Higher than 1 nm spectral resolution observations of the H Lyman $\alpha$ line needs to be undertaken from space in order to retrieve global quantitative information on the proton aurora. In addition, rocket campaigns dedicated to the comprehensive observation of proton aurora are required, as no strongly constrained validation of the H Lyman $\alpha$ line in proton aurora has been assessed to date.

[40] **Acknowledgments.** We are indebted to Harald Frey for his key input and helpful discussions regarding the IMAGE/FUV instruments. We thank Larry Paxton for providing us with the characteristics of the TIMED/GUVI instrument. M.G. efforts were supported by NASA grant NAG5-12773. D.L. was supported by NASA grant NAG5-12192.

[41] Arthur Richmond thanks Harald Frey and another reviewer for their assistance in evaluating this paper.

## References

Ajello, J. M. (1971), Dissociative excitation of $O_2$ in hte vacuum ultraviolet by electron impact, *J. Chem. Phys.*, *55*, 3156.

Ajello, J. M., and D. M. Shemansky (1985), A re-examination of important $N_2$ cross sections by electron impact with application to the dayglow: The Lyman-Birge-Hopfield band system and NI(119.99 nm), *J. Geophys. Res.*, *90*, 9845.

Anderson, P. C., D. L. McKenzie, M. Brittnacher, M. Chen, M. Hairston, and M. F. Thomsen (2000), Global storm time auroral X-ray morphology and timing and comparison with UV measurements, *J. Geophys. Res.*, *105*, 15,757.

Basu, B., J. R. Jasperse, R. M. Robinson, R. R. Vondrak, and D. S. Evans (1987), Linear transport theory of auroral proton precipitation: A comparison with observations, *J. Geophys. Res.*, *92*, 5920.

Basu, B., J. R. Jasperse, D. J. Strickland, and R. E. Daniell Jr. (1993), Transport-theoretic model for the electron-proton-hydrogen atom aurora, *J. Geophys. Res.*, *98*, 21,517.

Bertaux, J.-L., F. Goutail, and G. Kockarts (1984), Observations of Lyman-$\alpha$ emissions of hydrogen and deuterium, *Science*, *225*, 174.

Deehr, C., and D. Lummerzheim (2001), Ground-based optical observations of hydrogen emission in the auroral substorm, *J. Geophys. Res.*, *106*, 33.

Donovan, E. F., B. J. Jackel, I. Voronkov, T. Sotirelis, F. Creutzberg, and N. A. Nicholson (2003), Ground-based optical determination of the b2i boundary: A basis for an optical MT-index, *J. Geophys. Res.*, *108*(A3), 1115, doi:10.1029/2001JA009198.

Drob, D. P., R. R. Meier, J. M. Picone, D. J. Strickland, R. J. Cox, and A. C. Nicholas (1999), Atomic oxygen in the thermosphere during the July 13, 1982, solar proton event deduced from far ultraviolet images, *J. Geophys. Res.*, *104*, 4267.

Edgar, B. C., H. S. Porter, and A. E. S. Green (1975), Proton energy deposition in molecular and atomic oxygen and applications to the polar cap, *Planet. Space Sci.*, *23*, 787.

Frank, L. A., J. B. Sigwarth, J. D. Craven, J. P. Cravens, J. S. Dolan, M. R. Dvorsky, P. K. Hardebeck, J. D. Harvey, and D. W. Muller (1995), The Visible Imaging System (VIS) for the Polar spacecraft, *Space Sci. Res.*, *71*, 297.

Frey, H. U., S. B. Mende, C. W. Carlson, J.-C. Gerard, B. Hubert, J. Spann, R. Gladstone, and T. J. Immel (2001), The electron and proton aurora as seen by IMAGE-FUV and Fast, *Geophys. Res. Lett.*, *28*, 1135.

Frey, H. U., S. B. Mende, T. J. Immel, S. A. Fuselier, E. S. Claflin, J.-C. Gerard, and B. Hubert (2002), Proton aurora in the cusp, *J. Geophys. Res.*, *107*(A7), 1091, doi:10.1029/2001JA900161.

Frey, H. U., S. B. Mende, S. A. Fuselier, T. J. Immel, and N. Østgaard (2003a), Proton aurora in the cusp during southward IMF, *J. Geophys. Res.*, *108*(A7), 1277, doi:10.1029/2003JA009861.

Frey, H. U., S. B. Mende, T. J. Immel, J.-C. Gerard, B. Hubert, S. Habraken, J. Spann, G. R. Gladstone, D. V. Bisikalo, and V. I. Shematovich (2003b), Summary of quantitative interpretation of IMAGE far ultraviolet auroral data, *Space Sci. Rev.*, *109*, 255.

Fuller-Rowell, T. J., and D. S. Evans (1987), Height-integrated Pedersen and Hall conductivity patterns inferred from the TIROS-NOAA satellite data, *J. Geophys. Res.*, *92*, 7606.

Galand, M. (1996), Transport des protons dans l'ionosphere aurorale, Ph.D. thesis, Univ. Grenoble I, Grenoble, France.

Galand, M., and A. D. Richmond (2001), Ionospheric electrical conductances produced by auroral proton precipitation, *J. Geophys. Res.*, *106*, 117.

Galand, M., J. Lilensten, W. Kofman, and R. B. Sidje (1997), Proton transport model in the ionosphere: 1. Multistream approach of the transport equations, *J. Geophys. Res.*, *102*, 22,261.

Galand, M., R. Roble, and D. Lummerzheim (1999), Ionization by energetic protons in Thermosphere-Ionosphere Electrodynamics-General Circulation Model, *J. Geophys. Res.*, *104*, 27,973.

Galand, M., T. J. Fuller-Rowell, and M. V. Codrescu (2001), Response of the upper atmosphere to auroral protons, *J. Geophys. Res.*, *106*, 127.

Galand, M., D. Lummerzheim, A. W. Stephan, B. C. Bush, and S. Chakrabarti (2002), Electron and proton aurora observed spectroscopically in the far ultraviolet, *J. Geophys. Res.*, *107*(A7), 1129, doi:10.1029/2001JA000235.

Galand, M., J. Baumgardner, S. Chakrabarti, U. P. Løvhaug, B. Isham, J. Jussila, D. Lummerzheim, D. Evans, and F. Rich (2003), Proton aurora over EISCAT: Optical signature and associated ionospheric perturbations, in *Proceedings of 30th Annual Meeting on Atmospheric Studies by Optical Methods, August 13–17, 2003*, edited by F. Sigernes and D. A. Lorentzen, Univ. Courses on Svalbard Publ., Longyearbyen, Norway.

Germany, G. A., G. K. Parks, M. Brittnacher, J. Cumnock, D. Lummerzheim, J. F. Spann, L. Chen, P. G. Richards, and F. J. Rich (1997), Remote determination of auroral energy characteristics during substorm activity, *Geophys. Res. Lett.*, *24*, 995.

Gibson, S. T., H. P. F. Gies, A. J. Blake, D. G. McCoy, and P. J. Rogers (1983), Temperature dependence in the Schumann-Runge photoabsorption continuum of oxygen, *J. Quant. Spectrosc. Radiat. Transfer*, *30*, 385.

Hardy, D. A., M. S. Gussenhoven, and R. Raistrick (1987), Statistical and functional representations of the pattern of auroral energy flux, number flux, and conductivity, *J. Geophys. Res.*, *92*, 12,275.

Hardy, D. A., M. S. Gussenhoven, and D. Brautigam (1989), A statistical model of auroral ion precipitation, *J. Geophys. Res.*, *94*, 370.

Hedin, A. E. (1991), Extension of the MSIS thermosphere model into the middle and lower atmosphere, *J. Geophys. Res.*, *96*, 1159.

Immel, T. J., S. B. Mende, H. U. Frey, L. M. Peticolas, C. W. Carlson, J.-C. Grard, B. Hubert, S. A. Fuselier, and J. L. Burch (2002), Precipitation of auroral protons in detached arcs, *Geophys. Res. Lett.*, *29*(11), 1519, doi:10.1029/2001GL013847.

Ishimoto, M., C.-I. Meng, G. J. Romick, and R. E. Huffman (1989), Doppler shift of auroral Lyman $\alpha$ observed from a satellite, *Geophys. Res. Lett.*, *16*, 143.

Lanchester, B. S., M. Galand, S. C. Robertson, M. H. Rees, D. Lummerzheim, I. Furniss, L. M. Peticolas, H. U. Frey, J. Baumgardner, and M. Mendillo (2003), High resolution measurements and modeling of auroral hydrogen emission line profiles, *Ann. Geophys.*, *21*, 1629.

Lewis, B. R., L. Berzins, J. H. Carver, S. T. Gibson, and D. G. McCoy (1985), Decomposition of the photoabsorption continuum underlying the Schumann-Runge bands of ($^{16}O_2$). I-Role of the $B^3\Sigma_u^-$ state: A new dissociation limit, *J. Quant. Spectrosc. Radiat. Transfer*, *33*, 627.

Lilensten, J., and M. Galand (1998), Proton-electron precipitation effects on the electron production and density above EISCAT (Tromsø) and ESR, *Ann. Geophys.*, *16*, 1299.

Lorentzen, D. A., F. Sigernes, and C. S. Deehr (1998), Modeling and observations of dayside auroral hydrogen emission Doppler profiles, *J. Geophys. Res.*, *103*, 17,479.

Lu, G., et al. (1998), Global energy deposition during the January 1997 magnetic cloud event, *J. Geophys. Res.*, *103*, 11,685.

Lu, G., M. Brittnacher, G. Parks, and D. Lummerzheim (2000), On the magnetospheric source regions of substorm-related field-aligned currents and auroral precipitation, *J. Geophys. Res.*, *105*, 18,483.

Lummerzheim, D., and M. Galand (2001), The profile of the hydrogen H$\beta$ emission line in proton aurora, *J. Geophys. Res.*, *106*, 23.

Lummerzheim, D., and J. Lilensten (1994), Electron transport and energy degradation in the ionosphere: Evaluation of the numerical solution, comparison with laboratory experiments and auroral observations, *Ann. Geophys.*, *12*, 1039.

Lummerzheim, D., M. H. Rees, and H. R. Anderson (1989), Angular dependent transport of auroral electrons in the upper atmosphere, *Planet. Space Sci.*, *37*, 109.

Lummerzheim, D., M. Brittnacher, D. Evans, G. A. Germany, G. K. Parks, M. H. Rees, and J. F. Spann (1997), High time resolution study of the

hemispheric power carried by energetic electrons into the ionosphere during the May 19/20, 1996 auroral activity, *Geophys. Res. Lett.*, *24*, 987.
Lummerzheim, D., M. Galand, J. Semeter, M. J. Mendillo, M. H. Rees, and F. J. Rich (2001), Emission of OI (630 nm) in proton aurora, *J. Geophys. Res.*, *106*, 141.
Mende, S. B., et al. (2000), Far ultraviolet imaging from the IMAGE spacecraft, *Space Sci. Rev.*, *91*, 287.
Mende, S. B., H. U. Frey, M. Lampton, J.-C. Gerard, B. Hubert, S. Fuselier, J. Spann, R. Gladstone, and J. L. Burch (2001), Global observations of proton and electron auroras in a substorm, *Geophys. Res. Lett.*, *28*, 1139.
Mohan, H. (1979), Molecules of significance in planetary aeronomy, *Ref. Publ. 1030*, NASA, Washington, D. C.
Ogawa, S., and M. Ogawa (1975), Absorption cross sections of $O_2$ ($a^1\Delta_g$) and $O_2$ ($X^3\Sigma_g$) in the region from 1087 to 1700 Å, *Can. J. Phys.*, *53*, 1845.
Østgaard, N., et al. (2000), Global X-ray emission during an isolated substorm: A case study, *J. Atmos. Sol. Terr. Phys.*, *62*, 889.
Paresce, F., S. Chakrabarti, S. Bowyer, and R. Kimble (1983), The extreme ultraviolet spectrum of dayside and nightside aurorae: 800-1400 Å, *J. Geophys. Res.*, *88*, 4905.
Paxton, L. J., et al. (1999), Global ultraviolet imager (GUVI): Measuring composition and energy inputs for the NASA Thermosphere Ionosphere Mesosphere Energetics and Dynamics (TIMED) mission, *SPIE Opt. Spectrosc. Tech. Instrum. Atmos. Space Res. III*, *3756*, 265.
Paxton, L. J., D. Morrison, H. Kil, Y. Zhang, B. S. Ogorzalek, and C. Meng (2002), Validation of remote sensing products produced by the Special Sensor Ultraviolet Scanning Imager (SSUSI): A far UV imaging spectrograph on DMSP F-16, *SPIE Opt. Spectrosc. Tech. Instrum. Atmos. Space Res. IV*, *4485*, 338.
Petrinec, S. M., W. L. Imhof, D. L. Chenette, J. Mobilia, and T. J. Rosenberg (2000), Dayside/nightside auroral X-ray emission differences: Implications for ionospheric conductance, *Geophys. Res. Lett.*, *27*, 3277.
Rees, M. H., D. Lummerzheim, and R. G. Roble (1995), Modeling of the atmosphere-magnetosphere-ionosphere system MAMI, *Space Sci. Rev.*, *71*, 691.
Robinson, R. M., R. R. Vondrak, K. Miller, T. Dabbs, and D. Hardy (1987), On calculating ionospheric conductances from the flux and energy of precipitating electrons, *J. Geophys. Res.*, *92*, 2565.
Senior, C., J. R. Sharber, O. de la Beaujardire, R. A. Heelis, D. S. Evans, J. D. Winningham, M. Sugiura, and W. R. Hoegy (1987), E and F region study of the evening sector auroral oval: A Chatanika/Dynamics Explorer 2/NOAA 6 comparison, *J. Geophys. Res.*, *92*, 2477.
Senior, C. (1991), Solar and particle contributions to auroral height-integrated conductivities from EISCAT data: A statistical study, *Ann. Geophys.*, *9*, 449.
Sigernes, F. (1996), Estimation of initial auroral proton energy fluxes from Doppler profiles, *J. Atmos. Terr. Phys.*, *58*, 1871.
Søraas, F., H. R. Lindalen, K. Måseide, A. Egeland, T. A. Sten, and D. S. Evans (1974), Proton precipitation and the $H_\beta$ emission in a postbreakup auroral glow, *J. Geophys. Res.*, *79*, 1851.
Starr, W. L. (1976), Absorption cross sections of some atmospheric molecules for resonantly scattered OI 1304-Å radiation, *J. Geophys. Res.*, *81*, 3363.
Strickland, D. J., R. E. Daniell Jr., J. R. Jasperse, and B. Basu (1993), Transport-theoretic model for the electron-proton-hydrogen atom aurora: 2. Model results, *J. Geophys. Res.*, *98*, 21,533.
Strickland, D. J., R. J. Cox, R. R. Meier, and D. P. Drob (1999), Global O/N2 derived from DE 1 FUV dayglow data: Technique and examples from two storm periods, *J. Geophys. Res.*, *104*, 4251.
Strickland, D. J., J. Bishop, J. S. Evans, T. Majeed, R. J. Cox, D. Morrison, G. J. Romick, J. F. Carbary, L. J. Paxton, and C.-I. Meng (2001), Midcourse Space Experiment/Ultraviolet and Visible Imaging and Spectrographic Imaging limb observations of combined proton/hydrogen/electron aurora, *J. Geophys. Res.*, *106*, 65.
Torr, M. R., et al. (1995), A far ultraviolet imager for the international solar-terrestrial physics mission, *Space Sci. Rev.*, *71*, 329.
Vallance Jones, A. (1974), *Aurora*, D. Reidel, Norwell, Mass.
Zipf, E. C., and P. W. Erdman (1985), Electron impact excitation of atomic oxygen: Revised cross sections, *J. Geophys. Res.*, *93*, 11,087.

M. Galand, Center for Space Physics, Boston University, 725 Commonwealth Avenue, Boston, MA 02215, USA. (mgaland@bu.edu)
D. Lummerzheim, Geophysical Institute, University of Alaska, Fairbanks, AK 99775-7320, USA. (lumm@gi.alaska.edu)